TSUNAMI RUN-UP CONSIDERING TIME VARIATION OF DENSITY OF INUNDATION WATER

Hideo Matsutomi[1] and Taro Arikawa[2]

Aiming for the advancement of tsunami load, historical and/or prospective tsunami scale evaluations, practical empirical formulas for evaluating friction factor K of inundation flow and density ρ of inundation water over a movable bed, which can be applied to a tsunami run-up theory, are proposed using experimental data whose amount (range) is increased (expanded) by carrying out additional experiments on ρ and run-up of inundation flow with sediment, and verification data of the above theory under a uniformly sloping movable bed condition are provided. Series solutions with a higher universality to the run-up of tsunami inundation flow with sediment over a uniformly sloping movable bed, in which both K and ρ depend on time, are derived under the conditions depending on an incident bore height h_1 at shoreline (or an initial stored water depth), bed slope i, median particle diameter d_{50} of initial bed material, and examples of the solutions are shown. The solutions are applicable to the case that ρ is independent on time, i.e., the case of inundation flow without sediment over a movable bed or fixed bed. Including the case of inundation flow without sediment, validity of one of the solutions is also verified through a comparison with the verification data on run-up distance.

Keywords: tsunami; run-up theory; density of inundation water; friction factor of inundation flow with sediment

INTRODUCTION

Author et al. examined 1) dependencies of density ρ of inundation water and friction factor K of inundation flow over a movable bed on both incident Froude number F_{ri} of inundation flow and median particle diameter d_{50} of initial bed material experimentally (Matsutomi and Kawashima 2015; Matsutomi et al. 2016; Matsutomi et al. 2018; Matsutomi and Konno 2018; Matsutomi et al. 2019; Matsutomi 2019) and 2) effects of ρ and K on a tsunami run-up theoretically (Matsutomi 2020). However, the former 1) was examined under the condition of a small amount of experimental data (Exp. 1) and the latter 2) was done under the conditions that K depended on time and ρ was constant value comparable to average value in the run-up process (Theory II) and that both K and ρ were constant value comparable to average value in the run-up process (Theory III). Essentially, ρ depends on K. (Matsutomi 2019).

In light of the above situations, the present study aims to propose 1) empirical formulas for evaluating friction factor K of inundation flow and density ρ of inundation water over a movable bed, which can be applied to a tsunami run-up theory (Matsutomi 2020), using experimental data whose amount (range) is increased (expanded) by carrying out additional experiments (Exp. 2) on ρ and run-up of inundation flow with sediment, and 2) series solutions with a higher universality to the run-up of tsunami inundation flow with sediment over a uniformly sloping movable bed, in which both K and ρ depend on time, under the conditions depending on an incident bore height h_1 at shoreline (or an initial stored water depth), bed slope i, median particle diameter d_{50} of initial bed material (Theory I).

EXPERIMENT

Experimental Method

Experimental equipment. Experimental flume with 0.3 m in width is a handmade open channel of slide type, which can easily generate inundation flow with high Froude and Shields numbers. A horizontal flume to spread an experimental bed material (sand or silt) is attached to the downstream end of the slide slope with the inclination S_1. In addition, a short mild upslope with the inclination S_2 is attached to the downstream end of the horizontal flume to catch a proper amount of inundation water with sediment with a water receiving tank consisting of four (2 in a flow direction, 2 in a crossing direction) pieces of water tank of cube 0.3 m on each side, placed apart from the downstream (high side) end of the short mild upslope. A curved surface part is set up to smoothly connect the slide slope to the horizontal flume. In the experiment on tsunami run-up, a long mild upslope with the inclination S_2, whose surface is pasted sands of 0.85 to 2.0 mm in diameter to increase surface roughness, is even more attached to the downstream end of the short mild upslope. Outline of the experimental flume, its frontal view (right), arrangement of the measuring instruments (water receiving tank, wave gauges) and

[1] Research and Development Initiative, Chuo University, 1-13-27 Kasuga, Bunkyo-ku, Tokyo, 112-8551, Japan
[2] Civil and Environmental Engineering, Chuo University, 1-13-27 Kasuga, Bunkyo-ku, Tokyo, 112-8551, Japan

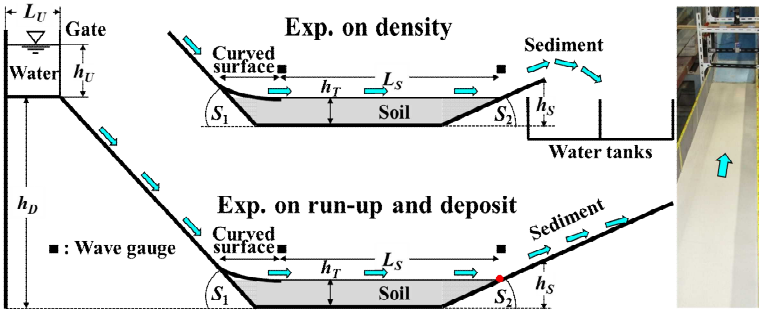

Figure 1. Outline of experimental flume (sidewalls are omitted), its frontal view (right), arrangement of measuring instruments and definition of symbols.

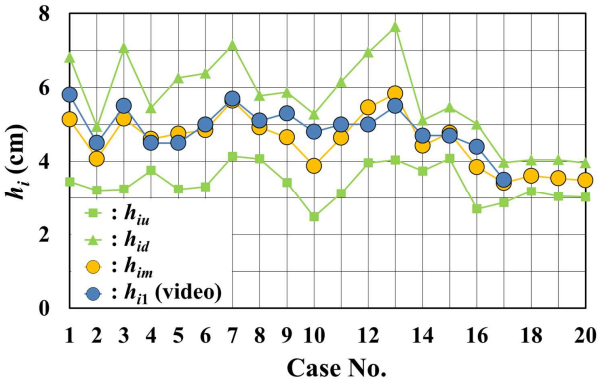

Figure 2. Comparison between incident inundation water depths h_i evaluated by the two methods (excluding the case of clear water).

definition of symbols are shown in Figure 1, where sidewalls of the flume are omitted, h_D is a height from the reference level to the bottom of water storage tank with 0.5 m in height, 0.3 m in width and 1.7 m in length, which is horizontally mounted on the top of the slide, h_U and L_U water depth and length stored in the water storage tank respectively, L_S an initial length of the spread bed material (or movable bed) zone, h_T an initial thickness of the spread bed material layer and h_S a height from the reference level to the downstream end of the short mild upslope.

Inundation flow is generated by rapidly pulling up a gate equipped to the water storage tank. The gate is located at the right end of the top of the slide as shown in Figure 1.

Measurement of hydraulic quantities. Two ultrasonic wave gauges (KEYENCE, UD-500) are installed at the upstream and the downstream ends of the initial movable bed zone respectively to measure time histories of incident inundation water depth as shown in Figure 1. The distance L_s between the two wave gauges ranges 2.76-3.01 m. The heights of the bed surface at the two ends are the same. The sampling time interval of the inundation water depths is 0.01 s.

Scales are stuck on one side vertically and both crests (see the frontal view picture in Figure 1) of sidewalls, and videos are taken from the one side and the top of the horizontal flume except for the cases of clear water to observe inundation flow situation and to evaluate incident inundation water depth and moving velocity of the tip position of inundation flow at the central part of the initial movable bed zone.

Incident inundation water depth h_i and incident Froude number $F_{ri}=u_i/\sqrt{gh_i}$ of inundation flow at the central part of the initial movable bed zone in the present experiment (Exp. 2) are evaluated by the following two methods, where u_i is an incident inundation flow velocity and g the gravitational acceleration. First method is the one using mean value h_{im} of the maximum incident inundation water depths h_{iu} and h_{id} in respective time histories measured at the two ends as h_i and mean moving velocity of the tip position of inundation flow evaluated by analysis of recorded video (in the case of clear water, recorded time histories of incident inundation water depth at the two ends) as u_i. Second method is the one using the maximum incident inundation water depth h_{i1} and mean moving velocity of the tip position of inundation flow evaluated by analysis of recorded videos. In the present experiment, the first method is adopted. The second method adopted in the previous experiment (Exp. 1) is used to check the validity of the first method.

Figure 2 shows a comparison between incident inundation water depths h_i (h_{im}, h_{i1}) evaluated by the first and second methods respectively. It can be seen from the figure that the incident inundation water depths evaluated by the two methods are almost the same.

Analysis Method

Experiment on density of inundation water. Inundation flow goes down the slide slope with the inclination S_1, takes in the bed material spread in the horizontal flume, runs up the short mild upslope with the inclination S_2 attached to the downstream end of the horizontal flume and then jumps out into the air (see Figure 1). After jumping out into the air, most inundation water with sediment is caught with the water receiving tank consisting of four pieces of water tank of cube 0.3 m on each side, which is placed apart from the downstream (high side) end of the short mild upslope. Weighed each water tank both beforehand and after inundation flow with sediment jumped into, mean density of inundation water caught can be evaluated because of that volume of the inundation water caught in each water tank can be evaluated by measuring water depth at four corners of filling water tank.

Experiment on run-up of inundation flow. Inundation flow taken in the bed material spread in the horizontal flume runs up and recedes over the long mild upslope with the inclination S_2 (see Figure 1). Inundated zone on the long mild upslope after run-up and backwash of inundation flow with sediment is divided into two zones (Matsutomi and Konno 2018). One is a tongue-shaped sedimentation zone. The other is its downstream (high side) zone where bed surface of the long mild upslope is just a little soiled with sediment. Therefore, it is defined that L_{RS} is the maximum distance of the tongue-shaped sedimentation zone, L_R and L_{RW} are respectively run-up distances of inundation flow with and without sediment over the long mild upslope starting at the downstream end (red dot point in Figure 1) of the initial movable bed zone. In this way, it is assumed that change of run-up phenomenon in a cross direction of the long mild upslope is small. Run-up experiment under the condition that the bed material is spread over the long mild upslope in advance is also carried out.

Experimental Conditions

Experimental conditions are summarized in Table 1, where M_{SD} is total mass of bed material initially spread in the horizontal flume in each experimental case. Commercial silica sand or silt, or natural sand collected on a natural coast is used as the bed material which is cooled down naturally after drying with a drying oven and is evenly spread in the horizontal flume without taking any special measures of compaction and others. Case 4 is a reference experiment because median particle diameter d_{50} of silt used is indefinite, though its officially published value exists (Kise and Arikawa 2020).

Table 1. Experimental conditions on density and run-up of Inundation flow with or without sediment (Exp. 2).

Case No.	h_D (m)	L_U (m)	h_U (m)	S_1 (°)	L_S (m)	h_T (m)	h_S (m)	S_2 (°)	M_{SD} (kg)	Remarks
1	0.34	1.7	0.25	5.1	3.01	0.06	0.11	7.4	82.8	Silica sand
2									88.8	
3									84.8	
4									35.5	Silt
5									85.2	Natural sand
6									82.4	
7									73.0	
8									96.2	
9	0.34	1.7	0.20	5.1	3.01	0.06	0.11	7.4	87.2	Natural sand
10									86.6	
11									88.2	
12	0.34	1.7	0.25	5.1	3.01	0.06	0.11	7.4	82.8	Silica sand
13									85.2	Natural sand
14									82.4	
15									90.1	
15a					2.77				130.6	
16	0.34	1.7	0.20	5.1	3.01	0.06	0.11	7.4	86.6	Natural sand
16a					2.76				122.7	
17					3.01				88.2	
17a					2.76				111.7	
18	0.34	1.7	0.25	5.1	3.01	0	0.11	7.4	0	Clear water
19										
20										

Table 2. Experimental results on density and run-up of Inundation flow with or without sediment (Exp. 2).

Case No.	d_{50} (mm)	U.C. (-)	C.C. (-)	h_i (cm)	F_{ri} (-)	P (g/cm^3)	L_R, L_{RW} (cm)	L_{RS} (cm)
1	0.16	1.55	0.90	5.14	2.19	1.134	-	-
2	0.76	1.96	0.90	4.08	2.50	1.024	-	-
3	0.29	2.62	0.73	5.16	2.23	1.112	-	-
4	-	-	-	4.61	2.36	1.077	-	-
5	0.21	1.92	0.87	4.75	2.28	1.128	-	-
6	0.23	2.00	0.76	4.85	2.22	1.121	-	-
7	0.11	-	-	5.65	2.20	1.110	-	-
8	0.50	2.08	1.03	4.93	2.26	1.042	-	-
9	0.22	2.08	0.85	4.65	2.19	1.105	-	-
10	0.35	1.73	1.01	3.88	2.18	1.037	-	-
11	0.33	2.19	1.30	4.65	1.99	1.044	-	-
12	0.16	1.55	0.90	5.46	2.02	-	207.0	198
13	0.21	1.92	0.87	5.84	1.99	-	185.5	174
14	0.23	2.00	0.76	4.43	2.40	-	196.5	177
15	0.50	2.08	1.03	4.89	2.24	-	243.4	112
15a	0.50	2.08	1.03	4.78	2.42	-	241.6	-
16	0.35	1.73	1.01	3.56	2.31	-	159.8	85
16a	0.35	1.73	1.01	3.85	2.17	-	168.5	-
17	0.33	2.19	1.30	3.75	2.17	-	179.5	91
17a	0.33	2.19	1.30	3.42	2.40	-	175.4	-
18	-	-	-	3.61	3.44	-	242.2	-
19	-	-	-	3.55	3.43	-	250.4	-
20	-	-	-	3.49	3.48	-	250.3	-

Case 15a, 16a, 17a are run-up experiment under the condition that the bed material with 0.03 m in initial layer thickness is spread over the long mild upslope with the inclination S_2 in advance. Grain size characteristics before beginning each experiment are shown in Table 2, where U.C. and C.C. are abbreviations of the uniformity and the curvature coefficients respectively. The number of times of experiment in each experimental case is once.

Experimental Results and Discussions

Table 2 shows a summary of experimental results. The density ρ of inundation water is evaluated from the total amount of inundation water trapped by the four water tanks. From the table, it can be surmised that ρ depends on both incident Froude number F_{ri} of inundation flow and median particle diameter d_{50} of initial bed material as well as previously reported (Matsutomi and Konno 2018).

Figure 3 shows a relationship between the incident Froude number F_{ri} and the density ρ/ρ_w of inundation water which are obtained in both the previous experiment (Exp. 1) and the present experiment (Exp. 2), where ρ_w is the density of clear water and these experimental data used are restricted to those obtained under the condition that the initial thickness of the spread bed material layer h_T is 0.06 m. In the figure, broken curve best fitted to each of three arbitrary present experimental data and friction factor K at the best fitted, which are based on Equation (1) described below, are indicated.

Experimental results on the run-up of inundation flow are discussed later (see Figure 12).

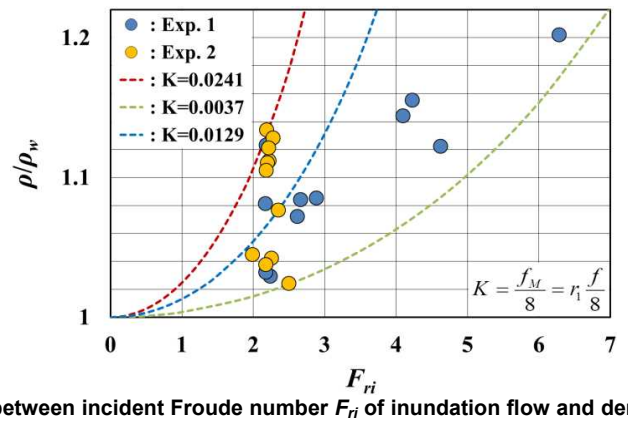

Figure 3. Relationship between incident Froude number F_{ri} of inundation flow and density ρ/ρ_w of inundation water (broken curves are based on Equation (1)).

EMPIRICAL FORMULAS

Matsutomi (2019) proposed the following relation between density ρ of inundation water and incident Froude number F_{ri} of inundation flow over a movable bed through a process of evaluating total sediment discharge:

$$\frac{\rho}{\rho_w} = 1\Big/\left(1-\frac{f_M}{8}F_{ri}^2\right) = 1\Big/\left(1-r_1\frac{f}{8}F_{ri}^2\right) = 1\Big/\left(1-KF_{ri}^2\right) \tag{1}$$

where f_M and f are friction factors of inundation flow and steady flow over a movable bed respectively, r_1 ratio f_M/f of the former friction factor to the latter friction factor (refer to the reference (Matsutomi 2019) with respect to evaluation method for each experimental value of r_1) and K ($=f_M/8=r_1f/8$) a newly defined friction factor of inundation flow over a movable bed (Matsutomi 2020). The following relation is adopted as a frictional resistance law for steady flow over a movable bed (Ashida 1959):

$$\frac{8}{f} = \left(6.0+5.75\log_{10}\frac{h_i}{3d_{50}}\right)^2 \tag{2}$$

where $3d_{50}$ is adopted as the equivalent sand roughness k_s.

Matsutomi (2019) also proposed the following preliminary empirical formula for r_1:

$$r_1 = 0.234F_{ri}^{-1.05}\left(\frac{h_i}{3d_{50}}\right)^{0.94} = 0.083F_{ri}^{-1.05}\left(\frac{h_i}{d_{50}}\right)^{0.94} \tag{3}$$

Figure 4 shows a comparison between experimental data of r_1 and Equation (3) (broken curves), where the experimental data include those obtained by the present experiment (Exp. 2) and the broken curves are obtained by substituting the upper and the lower limit values of experimental data ranges ($1.99<F_{ri}<6.29$, $54<h_i/d_{50}<513$) into Equation (3) respectively. In the figure, the following Equation (4) (solid curves) is also indicated, which can be applied to a tsunami run-up theory discussed in the next chapter and has almost the same accuracy as Equation (3).

$$r_1 = 0.327F_{ri}^{-1}\left(\frac{h_i}{3d_{50}}\right)^{0.807} = 0.135F_{ri}^{-1}\left(\frac{h_i}{d_{50}}\right)^{0.807} \tag{4}$$

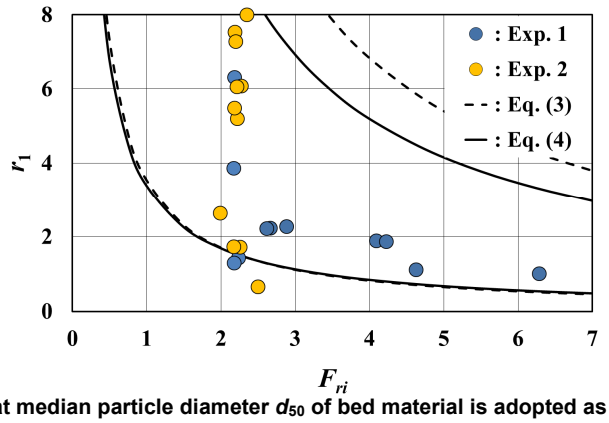

(a) Case that median particle diameter d_{50} of bed material is adopted as a parameter

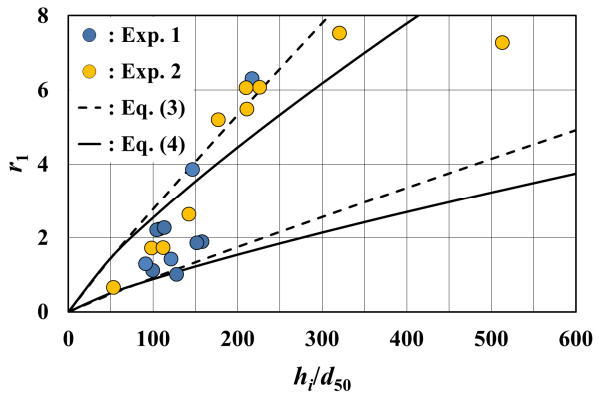

(b) Case that incident Froude number F_{ri} is adopted as a parameter

Figure 4. Comparison between experimental value and evaluated value by the two empirical formulas for the ratio r_1 ($=f_M/f$).

From Figure 4, it can be understood that 1) the experimental data are well contained in the region between the broken curves based on Equation (3), though some experimental data are out of the region, and 2) the experimental data are fairly well contained in the region between the solid curves based on Equation (4), though utility of Equation (4) is slightly inferior to that of Equation (3). Though proposing a new empirical formula for r_1 can be considered, it can't be recommended under the present situation of a small amount of experimental data.

When Equation (4) is adopted as r_1, friction factor K of inundation flow is expressed as Equation (5) in which power numbers become round numbers. Equation (5) enables to derive solutions to the tsunami run-up theory discussed in the next chapter.

$$\begin{aligned} K &= f_M/8 = r_1 f/8 \\ &= 0.327\left(6.0+5.75\log_{10}\frac{h_i}{3d_{50}}\right)^{-2} F_{ri}^{-1}\left(\frac{h_i}{3d_{50}}\right)^{0.807} \\ &\cong 0.00442 F_{ri}^{-1}\left(\frac{h_i}{3d_{50}}\right)^{0.5} = 0.00255 F_{ri}^{-1}\left(\frac{h_i}{d_{50}}\right)^{0.5} \end{aligned} \tag{5}$$

where the following approximate relation which can be applicable within the experimental data range ($54<h_i/d_{50}<513$) is used:

$$\left(6.0+5.75\log_{10}\frac{h_i}{3d_{50}}\right)^{-2} \cong 0.0135\left(\frac{h_i}{3d_{50}}\right)^{-0.307} \tag{6}$$

Figure 5 shows the approximation degree of Equation (6). The determination coefficient R^2 is 0.999.

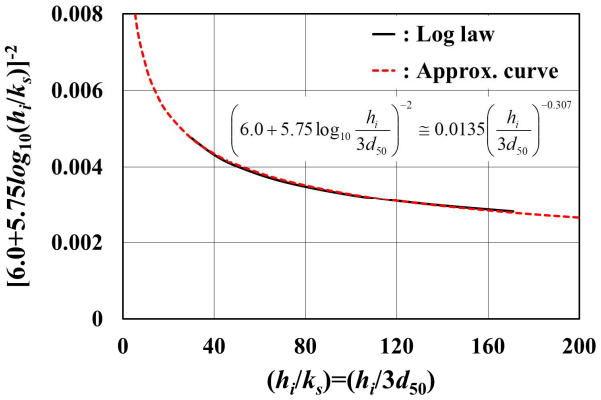

Figure 5. Approximate curve (red broken line) for frictional resistance law (black solid line) of steady flow over a movable bed.

Therefore, Equation (7) as a practical empirical formula for evaluating the density ρ of inundation water over a movable bed can be obtained from Equations (1) and (5):

$$\frac{\rho_w}{\rho} = 1 - 0.00255 F_{ri}\left(\frac{h_i}{d_{50}}\right)^{0.5} \tag{7}$$

where incident Froude number F_{ri} of inundation flow must be less than around $247\sqrt{d_{50}/h_i}$ which stems from the density (=2.7 g/cm^3) of bed material. Equation (7) indicates that 1) ρ can also be considered as depending on both incident inundation flow velocity u_i and median particle diameter d_{50} of initial bed material and 2) when F_{ri} and incident inundation water depth h_i are a function of time, ρ and K are also a function of time, respectively.

On the other hand, Equation (8) can be obtained from Equations (1), (2), (3) and (6):

$$\frac{\rho_w}{\rho} = 1 - 0.00158 F_{ri}^{0.95}\left(\frac{h_i}{d_{50}}\right)^{0.633} \tag{8}$$

Figure 6 shows a comparison between Equations (7) and (8) together with the experimental data of ρ/ρ_w. As well as Figure 4, the upper and the lower limit values of the experimental data ranges are respectively adopted as the value of each parameter in the two equations. From Figure 6, it can be understood that though some experimental data are out of each region between the solid or broken curves based on Equation (7) or (8), both equations are fairly well practical empirical formulas for evaluating the density ρ of inundation water over a movable bed.

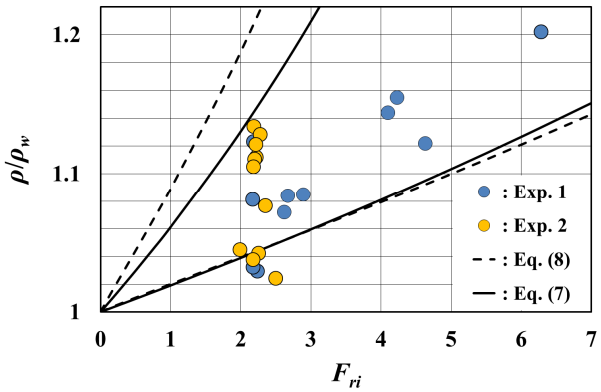

(a) Case that median particle diameter d_{50} of bed material is adopted as a parameter

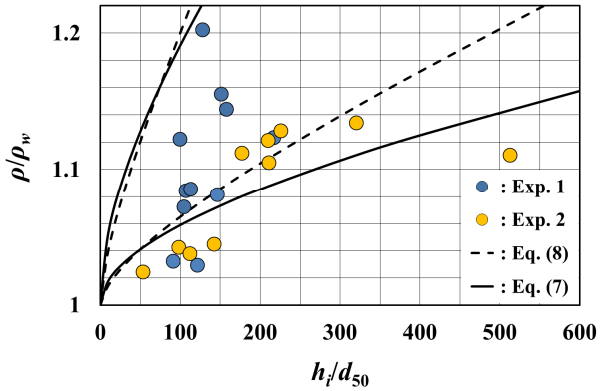

(b) Case that incident Froude number F_{ri} is adopted as a parameter

Figure 6. Comparison between experimental value $(\rho/\rho_w)_e$ and evaluated value $(\rho/\rho_w)_m$ by the two empirical formulas for the density of inundation water.

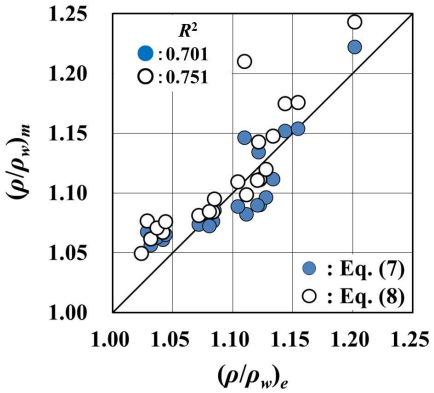

Figure 7. Comparisons between experimental value $(\rho/\rho_w)_e$ and evaluated value $(\rho/\rho_w)_m$ by two empirical formulas for density of inundation water, where R^2 is the determination coefficient.

Figure 7 shows a comparison between experimental value $(\rho/\rho_w)_e$ and evaluated value $(\rho/\rho_w)_m$ by each practical empirical formula for the density ρ, of inundation water. From the figure, it can be understood that 1) agreement between the experimental value and the evaluated value by each practical empirical formula is relatively well (R^2 is 0.701 and 0.751 in turn), 2) both practical empirical formulas have almost the same agreement.

RUN-UP THEORY

A run-up theory of tsunami inundation flow with sediment over a movable bed with a uniform slope i is developed under a more practical condition that 1) sediment median particle diameter d_{50} of initial bed material is constant and 2) both friction factor K of inundation flow and density ρ of inundation water depend on time.

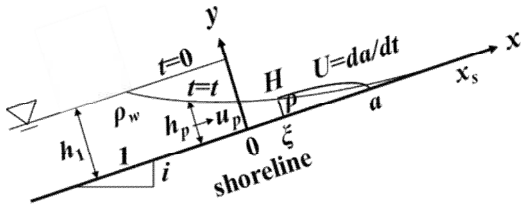

Figure 8. Outline of Initial condition and definition of main symbols.

Figure 8 shows an outline of bed topography, initial condition, coordinate system (x, y) and definition of main symbols of tsunami inundation flow, where h_1 is incident bore height at shoreline x=0 (or initial stored water depth), t time, x distance axis along the bed, x_s tip position in the case of no friction, h_p and u_p inundation water depth and inundation flow velocity at x=x in the case of no friction respectively, $\xi(t)$ rear position of the tip region, H inundation water depth at x=ξ, $a(t)$ the tip position of inundation flow with sediment and U inundation flow velocity in the tip region. When a hydraulic resistance is introduced in the tip region (=$a(t)$-$\xi(t)$) of inundation flow and inundation flow velocity U (=da/dt) in the tip region is assumed to be a function of time alone, the basic equation to the tip region under the hydrostatic pressure approximation is (Matsutomi 2020):

$$\left(c_1-\frac{1}{2}\frac{da}{dt}-\frac{1}{2}igt\right)^3 t\frac{d^2a}{dt^2}-\frac{1}{2}\frac{\rho_w}{\rho}\left(c_1-\frac{1}{2}\frac{da}{dt}-\frac{1}{2}igt\right)^4 + ig\left(c_1-\frac{1}{2}\frac{da}{dt}-\frac{1}{2}igt\right)^3 t+Kg\left\{a-\left(\frac{3}{2}\frac{da}{dt}-c_1+igt\right)t\right\}\left(\frac{da}{dt}\right)^2=0 \tag{9}$$

where c_1=$\sqrt{gh_1}$ and a threshold of bed material movement is not introduced.

After applying the empirical formula for ρ_w/ρ obtained by replacing h_i in Equation (7) with H which is expressed by Equation (10) (Matsutomi 2020) to ρ_w/ρ in Equations (9) and (11) (Matsutomi 2020),

$$H=\frac{1}{g}\left(c_1-\frac{1}{2}\frac{da}{dt}-\frac{1}{2}igt\right)^2 \tag{10}$$

$$K=\left(1-\frac{\rho_w}{\rho}\right)\frac{1}{F_{ri}^2}=\left(1-\frac{\rho_w}{\rho}\right)\frac{(2c_1-da/dt-igt)^2}{4(da/dt)^2} \tag{11}$$

and then by rewriting friction factor K in Equation (9) with the rewritten Equation (11) above stated, the following Equation (12) can be obtained:

$$\left(c_1-\frac{1}{2}\frac{da}{dt}-\frac{1}{2}igt\right)t\frac{d^2a}{dt^2}-\frac{1}{2}\left(1-\frac{0.00255}{\sqrt{gd_{50}}}\frac{da}{dt}_*\right)\left(c_1-\frac{1}{2}\frac{da}{dt}-\frac{1}{2}igt\right)^2 + ig\left(c_1-\frac{1}{2}\frac{da}{dt}-\frac{1}{2}igt\right)t+\frac{0.00255g}{\sqrt{gd_{50}}}\left\{a-\left(\frac{3}{2}\frac{da}{dt}-c_1+igt\right)t\right\}\frac{da}{dt}=0 \tag{12}$$

Equation (12) which depends on incident bore height h_1 at shoreline, bed slope i, median particle diameter d_{50} of initial bed material is the basic equation in the present study and seems to have a higher universality compared with the previous basic equations (Matsutomi 2020) derived under the conditions of a constant density ρ of inundation water and a constant or a time-dependent friction factor K of inundation flow. Terms with the subscript $*$ in Equation (12) vanish when ρ/ρ_w=1 (clear water) corresponding to the case that the same frictional resistance force as the one acting on a movable bed acts on a fixed bed or frictional resistance force is within the maximum one acting on a movable bed under the static equilibrium condition. Meaning of the subscript $*$ is the same hereinafter.

To solve Equation (12), let us introduce the following new variables α and τ:

$$\alpha=\frac{1}{h_1}\left(2c_1t-\frac{1}{2}igt^2-a\right) \tag{13}$$

$$\tau=\sqrt{\frac{g}{h_1}}t \tag{14}$$

where α ($\geq$0) is a dimensionless distance between the tip positions $x_s(t)$ and $a(t)$ of inundation flow without and with sediment. By introducing these new variables, Equation (12) is rewritten as follows:

$$-\tau\frac{d\alpha}{d\tau}\left(\frac{d^2\alpha}{d\tau^2}\right)-\frac{1}{4}\left(\frac{d\alpha}{d\tau}\right)^2+\frac{\beta}{4}\left(\frac{d\alpha}{d\tau}\right)^2\left(2-i\tau-\frac{d\alpha}{d\tau}\right)_*+2\beta\left\{-\alpha+\frac{3}{2}\tau\frac{d\alpha}{d\tau}\right\}\left(2-i\tau-\frac{d\alpha}{d\tau}\right)=0 \tag{15}$$

where β=$0.00255\sqrt{h_1/d_{50}}$.

Further, let us introduce the following variable conversions:

$$p=\frac{d\alpha}{d\tau} \quad (16) \qquad \tau=f'(p)=\frac{df}{dp} \quad (17)$$

where p ($\geq$0) indicates a dimensionless velocity. These conversions lead to the following relations:

$$\frac{d^2\alpha}{d\tau^2}=\frac{1}{d^2f/dp^2} \quad (18) \qquad \alpha=p\frac{df}{dp}-f \quad (19)$$

Therefore, Equation (15) becomes the following ordinary differential equation for $f(p)$:

$$-pf'-\frac{1}{4}p^2f''+\frac{\beta}{4}\left(p^2{}_*+8f+4f'p\right)\left(2-if'-p\right)f''=0 \quad (20)$$

Let us assume that the dependent variable $f(p)$ can be expanded into a power series of p as follows:

$$f(p)=\sum_{n=0}^{\infty}b_np^n \quad (21)$$

From the initial conditions that $\alpha=d\alpha/dt=0$ ($p=0$) at $\tau=0$ ($t=0$), $b_0=b_1=0$ can be obtained. Substituting Equation (21) into Equation (20) considering the result $b_0=b_1=0$, the following identical equation is obtained:

$$\begin{aligned}&-\left(10b_2+18b_3p+28b_4p^2+40b_5p^3+54b_6p^4+....\right)p^2\\&+\beta\left(1_*+16b_2+20b_3p+24b_4p^2+28b_5p^3+32b_6p^4+....\right)\\&\times\begin{pmatrix}4b_2+\left(12b_3-2b_2-4ib_2^2\right)p+\left(24b_4-6b_3-18ib_2b_3\right)p^2\\+\left(40b_5-12b_4-32ib_2b_4-18ib_3^2\right)p^3+\left(60b_6-20b_5-50ib_2b_5-60ib_3b_4\right)p^4+....\end{pmatrix}p^2=0\end{aligned} \quad (22)$$

Solving the identical equation (22), Equations (23) to (27) are obtained as the coefficients b_2 to b_6:

$$b_2=\frac{5-2\beta_*}{32\beta} \quad (23) \qquad b_3=\frac{\beta\left(1_*+16b_2\right)\left(1+2ib_2\right)b_2}{2\beta\left(3_*+68b_2\right)-9} \quad (24)$$

$$b_4=\frac{\beta\left(3\left(1_*+16b_2\right)\left(1+3ib_2\right)-20\left(6b_3-b_2-2ib_2^2\right)\right)b_3}{12\beta\left(1_*+20b_2\right)-14} \quad (25)$$

$$b_5=\frac{\beta\left(\left(1_*+16b_2\right)\left(6b_4+16ib_2b_4+9ib_3^2\right)+60\left(1+3ib_2\right)b_3^2+24\left(1+2ib_2\right)b_2b_4-384b_3b_4\right)}{4\beta\left(5_*+94b_2\right)-20} \quad (26)$$

$$b_6=\frac{\beta\begin{pmatrix}5\left(1_*+16b_2\right)\left(2b_5+5ib_2b_5+6ib_3b_4\right)+20\left(6b_4+16ib_2b_4+9ib_3^2\right)b_3\\-24\left(12b_4-3b_3-9ib_2b_3\right)b_4+28\left(1+2ib_2\right)b_2b_5-568b_3b_5\end{pmatrix}}{2\beta\left(15_*+272b_2\right)-27} \quad (27)$$

From the above results, the following series solutions to the tip position $a(t)$, velocity $U(t)$ and acceleration d^2a/dt^2 of inundation flow with sediment over a uniformly sloping movable bed, which depend on h_1, i and d_{50}, can be obtained:

$$a=2c_1t-\frac{1}{2}igt^2-h_1\left(b_2p^2+2b_3p^3+3b_4p^4+4b_5p^5+5b_6p^6+....\right) \quad (28)$$

$$U=\frac{da}{dt}=2c_1-igt-c_1p \quad (29)$$

$$\frac{d^2a}{dt^2}=-ig-\frac{g}{2b_2+6b_3p+12b_4p^2+20b_5p^3+30b_6p^4+....} \quad (30)$$

$$t=\sqrt{\frac{h_1}{g}}\left(2b_2p+3b_3p^2+4b_4p^3+5b_5p^4+6b_6p^5+....\right) \quad (31)$$

Figure 9 shows an example of convergence of Equations (28) and (31) which are the series solution to the tip position $a(t)$ of inundation flow with sediment in the case that incident bore height h_1=0.09 m at shoreline, bed slope i=0.05, relative incident bore height h_1/d_{50}=300. It can be seen from the figure that adopting the 5th order approximate solution consisting of the coefficients b_2 to b_6, the series solution to $a(t)$ converges with enough accuracy, e.g., the difference between the 4th and 5th order approximate solution to the maximum run-up distance is around 2.4%. Therefore, the 5th order approximate solution is adopted hereinafter. Figure 9 also indicates that the trajectory of the tip position $a(t)$ in the run-up and the backwash processes is not axisymmetric.

Figure 10 shows an example of time histories of the tip position $a(t)$ of inundation flow, friction factor K of inundation flow in the tip region and density ρ/ρ_w of inundation water in the tip region under the conditions that h_1=0.09 m, i=0.05, h_1/d_{50}=300, where no restrictions are imposed on both the use of Equation (1) and the value of ρ/ρ_w. However, friction factor K in a final stage of the run-up and density

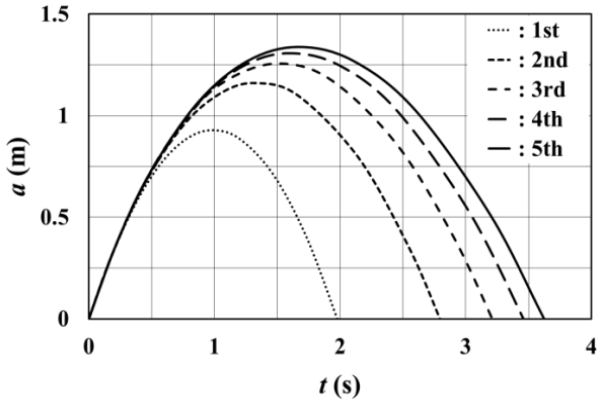

Figure 9. Convergence example of series solution to the tip position $a(t)$ of inundation flow (h_1=0.09 m, i=0.05, h_1/d_{50}=300).

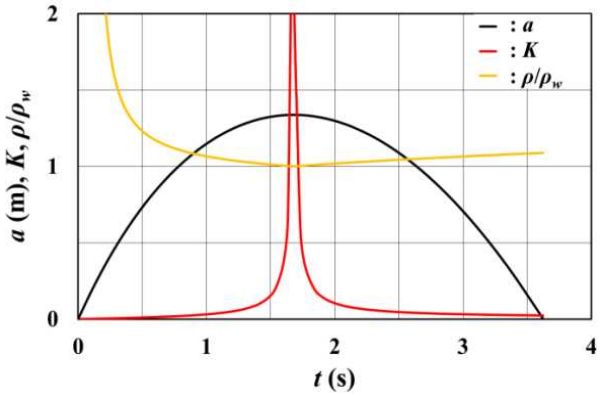

Figure 10. Time histories of the tip position $a(t)$ of inundation flow, friction factor K of inundation flow in the tip region and density ρ/ρ_w of inundation water in the tip region (5^{th} order approximation) (h_1=0.09 m, i=0.05, h_1/d_{50}=300).

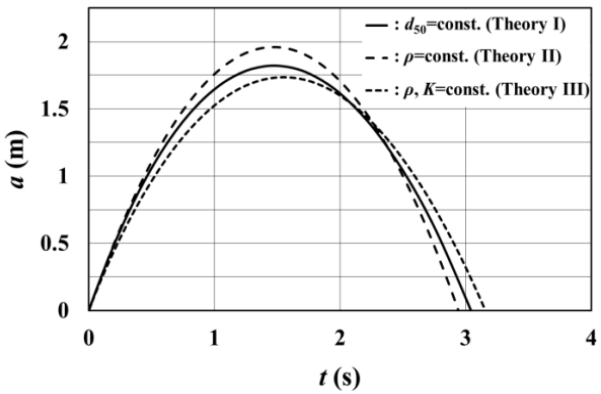

Figure 11. Comparison among time histories of the tip position $a(t)$ of inundation flow evaluated by Theory I, II and III (Case 12: h_1=0.1811 m, i=0.123, k_s=d_{50}=1.0 mm, ρ/ρ_w=1.036, K=0.00077).

ρ/ρ_w in an early stage of the run-up are omitted in the figure. Both Equation (1) and simplified run-up model, i.e., dam break flow model adopted in the present study are related to the omission. The former is due to that inundation flow velocity U (=da/dt) approaches to zero in the final stage. The latter is due to that incident Froude number F_{ri} of inundation flow approaches to infinity in the early stage. It can be seen from Figure 10 that both K and ρ/ρ_w depend on time.

Figure 11 shows a comparison among time histories of the tip position $a(t)$ evaluated by Theory I, II and III (Case 12: h_1=0.1811 m, i=0.123, k_s=d_{50}=1.0 mm, ρ/ρ_w=1.036, K=0.00077). Analytical solution to Theory II and series solution to Theory III to $a(t)$ are Equation (32) and Equations (33) to (39), respectively:

$$a = 2c_1 t - \frac{1}{2} igt^2 - 4\frac{(1-\rho_w/\rho)}{(4+\rho_w/\rho)} gt^2 \tag{32}$$

$$a = 2c_1 t - \frac{1}{2} igt^2 - \frac{h_1}{K}\left(3b_4 p^4 + 4b_5 p^5 + 5b_6 p^6 + 6b_7 p^7 + 7b_8 p^8 + ...\right) \tag{33}$$

$$t = \frac{1}{K}\sqrt{\frac{h_1}{g}}\left(4b_4 p^3 + 5b_5 p^4 + 6b_6 p^5 + 7b_7 p^6 + 8b_8 p^7 + ...\right) \tag{34}$$

where

$$b_4 = \frac{1}{1{,}152}\left(4 + 3\frac{\rho_w}{\rho}\right) \quad (35) \qquad b_5 = \frac{1{,}152 b_4^2}{\left(3{,}264 b_4 - 5 - 5\,\rho_w/\rho\right)} \quad (36) \qquad b_6 = \frac{64\left(9b_4^2 - 102 b_4 b_5 + 70 b_5^2\right)}{\left(12 + 15\,\rho_w/\rho - 8{,}832 b_4\right)} \quad (37)$$

$$b_7 = \frac{32\left(51 b_4 b_5 - 276 b_4 b_6 - 140 b_5^2 + 370 b_5 b_6 - 288 b_4^3\, i/K\right)}{\left(14 + 21\,\rho_w/\rho - 11{,}520 b_4\right)} \tag{38}$$

$$b_8 = \frac{8\left(69 b_4 b_6 - 360 b_4 b_7 + 35 b_5^2 - 370 b_5 b_6 + 474 b_5 b_7 + 240 b_6^2 + 24 b_4^2\left(6b_4 - 49 b_5\right) i/K\right)}{\left(4 + 7\,\rho_w/\rho - 3{,}648 b_4\right)} \tag{39}$$

In Figure 11, h_1=0.1811 m and i=0.123 are adopted in common, and h_1/d_{50}=188.1 in the present theory (Theory I), ρ/ρ_w=1.036 in Theory II, and ρ/ρ_w=1.036 and K=0.00077 in Theory III are adopted, where K and ρ are average values in the run-up process (Matsutomi 2022). From the figure, it can be seen that $a(t)$ evaluated by Theory I is positioned between those evaluated by Theory II and III. Median particle diameter d_{50} of bed material remains unchanged unless a mixed-sized particle is considered. Therefore, it seems to be judged that Theory I has the highest universality and is the most practical among the three theories, and Theory II and III have a tendency to evaluate run-up speed and height high and low respectively. The tendencies indicated by Theory II and III suggest that there is still room for improvement in the conventional approach (e.g., time-independent friction factor) to the tsunami run-up analyses including numerical ones.

VERIFICATION AND DISCUSSION

Validity of the series solution to the tip position $a(t)$ of inundation flow (Equations (28) and (31)) is verified through a comparison between experimental value L_{Re} (L_R or L_{RW} in Table 2) and theoretical value L_{Rt} of the maximum run-up distance. However, the comparison between experimental and theoretical values under the same condition is impossible at present because physical experiment under the same condition as that of the series solution is difficult and there are no experimental data yet.

In the series solution, Equation (40) is adopted as an initial stored water depth h_1 (Matsutomi 2022):

$$h_1 = h_{id} + u_i^2/2g \tag{40}$$

where inundation flow velocity u_i used in the incident Froude number F_{ri} of inundation flow can be evaluated from the experimental data in Table 2. Equivalent sand roughness k_s=d_{50}=1.0 mm (Matsutomi 2020) or k_s=3d_{50} (Case 15a-17a) is adopted for the fixed mild upslope bed, whose surface is pasted sands of 0.85-2.0 mm in diameter, with the inclination S_2 or a movable mild upslope bed with the inclination S_2.

Figure 12 shows a comparison between experimental value L_{Re} and theoretical value L_{Rt} of the

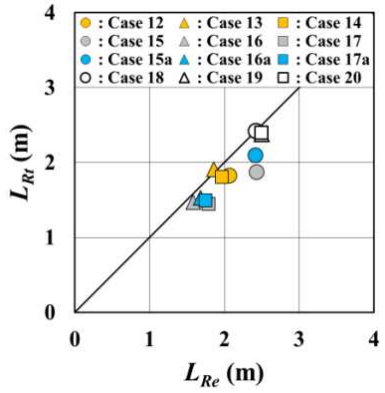

Figure 12. Comparison between experimental value L_{Re} and theoretical value L_{Rt} of the maximum run-up distance.

maximum run-up distance. Since agreement between the two is relatively well, it may be judged that validity of both the series solution to $a(t)$ and the method for evaluating h_1 is high.

CONCLUSIONS

Main results obtained by the present study are that:

1. Empirical formulas (Equations (5) and (7)) for evaluating friction factor K of inundation flow and density ρ of inundation water over a movable bed, which can be applied to tsunami run-up theory, were proposed (Figure 3), and verification data (the maximum run-up distance L_{Re}) of the theory under a uniformly sloping movable bed condition were provided (Table 2).
2. Series solutions with a higher universality (Equations (28)-(31)) to the run-up of inundation flow with sediment over a uniformly sloping movable bed, in which both K and ρ depended on time, were derived under the conditions depending on an incident bore height h_1 at shoreline, bed slope i, median particle diameter d_{50} of initial bed material. Examples and a comparison of the solution to the tip position $a(t)$ of inundation flow were also shown (Figures 9 -11).
3. Validity of the derived series solution to the maximum run-up distance L_{Rt} (Equations (28) and (31)) was confirmed through a comparison with the verification data stated above, including the case of inundation flow without sediment (Figure 12).

Finally, we wish to remark that Theory II can be applied to predict the water surface profile, sediment transport rate, etc. in the tip region of inundation flow with sediment.

ACKNOWLEDGMENTS

This work was supported by JSPS the Grant-in-Aid for Scientific Research (C) Grant Numbers JP20K05041.

REFERENCES

Ashida, K. 1959. Design method for river channel - on the roughness of river (4) -, *Civil engineering journal*, 1, 7, 8-11. (in Japanese)

Kise, K., and T. Arikawa. 2020. Experimental study on the influence of suspended silt and sand on tsunami force, *Journal of JSCE*, B2, 76, 2, 385-390. (in Japanese)

Matsutomi, H., and S. Kawashima. 2015. Elementary experiment on the maximum density of tsunami inundation flow, *Journal of JSCE*, B2, 71, 2, 355-360. (in Japanese)

Matsutomi, H., F. Konno, S. Saikawa, T. Kamataki, and K. Watanabe. 2016. Influence of the density of tsunami flooding water on tsunami deposit and run-up height, *Journal of JSCE*, B2, 72, 2, 397-402. (in Japanese)

Matsutomi, H., H. Okada, T. Kubota, and F. Konnno. 2018. Experiments on the dependency of tsunami load on RC building on the density of tsunami inundation water, *Journal of JSCE*, B2, 74, 2, 265-270. (in Japanese)

Matsutomi, H., and F. Konno. 2018 Experiments on the density of tsunami inundation water and its influence on the tsunami run-up and deposit, *Proc. of ICCE*, No.36, Paper.41.

Matsutomi, H., A. Mikami, and Y. Chiba. 2019. Influence of the tsunami inundation water density and wave period on the tsunami load on RC building, *Journal of JSCE*, B2, 75, 2, 397-402. (in Japanese)

Matsutomi, H. 2019. A simple method for evaluating the density of tsunami inundation water, *Journal of JSCE*, B2, 75, 2, 385-390. (in Japanese)

Matsutomi, H. 2020. Effect of the density of inundation water on tsunami run-up, *Proc. of vICCE*, Paper.62.

Matsutomi, H. 2022. Method for applying frictional resistance law of inundation flow over a movable bed to tsunami run-up, *Tohoku Journal of Natural Disaster Science*, 58, 57-62. (in Japanese)